Computational Modeling of Arterial Walls: Evaluating Model Complexity and the Influence of Model Parameters on Deformation Outcomes

Seda Aslan[1], Xiaolong Liu[2], Enze Chen[3], Miya Mese-Jones[4], Bryan Gonzalez[5], Ryan O'Hara[5], Yue-Hin Loke[5,6], Narutoshi Hibino[7], Laura Olivieri[8], Axel Krieger[1], Thao D. Nguyen[1]

[1]*Department of Mechanical Engineering, Johns Hopkins University, Baltimore, MD, U.S.A.*

[2]*Department of Mechanical Engineering, Texas Tech University, Lubbock, TX, U.S.A.*

[3]*Department of Civil and Systems Engineering, Johns University, Baltimore, MD, U.S.A.*

[4]*Baltimore Polytechnic Institute, Baltimore, MD, U.S.A.*

[5]*Sheikh Zayed Institute of Pediatric Surgical Innovation, Children's National Hospital, Washington DC, U.S.A.*

[6]*Division of Cardiology, Children's National Hospital, Washington DC, U.S.A*

[7]*Section of Cardiac Surgery, Department of Surgery, The University of Chicago Medicine, Chicago, IL, USA*

[8]*Division of Pediatric Cardiology, University of Pittsburgh Medical Center, Pittsburgh, PA, U.S.A.*

saslan2@jhu.edu, Xiaolong.Liu@ttu.edu, echen45@jhu.edu, miyaelisemj@gmail.com, BGONZALEZ, ROHARA,YLoke@childrensnational.org, nhibino@bsd.uchicago.edu, olivierilj@upmc.edu, axel,Vicky.Nguyen@jhu.edu

Keywords: Biomechanical Modeling, Arterial Wall Modeling, Patient-specific FE Models

Abstract: Computational models have been instrumental in advancing cardiovascular applications, particularly in simulating arterial behaviors for pre-surgical treatment strategies. Nonetheless, uncertainties arising from patient-specific parameters, such as arterial wall thickness and material properties, pose challenges to their precision. This study utilized finite element analysis to simulate the deformation response of the porcine pulmonary artery to a pressure change and performed a sensitivity analysis of the effects of material properties and vessel wall thickness on the deformation. The widely recognized Holzapfel-Gasser-Ogden (HGO) model was used to describe the stress-strain behavior of the arterial wall. Initially, the arterial walls were modeled as a single layer, then as separate adventitia and intima-media layers with constant thickness. The model complexity was increased by varying thickness and specific material properties of different regions in pulmonary arteries, based on *ex vivo* data from existing literature. For the sensitivity analysis, the HGO model parameters were adjusted within their measured variance to study their impact on deformation. The results showed that a single layer, regionally varying wall thickness is needed to reproduce the *in vivo* measure strain response of the cardiac cycle. The strain response was also most sensitive to variations in the thickness and isotropic shear modulus of the vessel wall. Using this knowledge, we tuned the model parameters for three porcine models until the deformation results were within 10% of the MRI-measured deformations. This study offers valuable insights to identify key model features for specimen-specific computational modeling of the pulmonary artery, thus providing a foundation for enhancing the realism of soft tissue deformation simulations.

1 INTRODUCTION

The importance of computational models cannot be overstated in the rapidly evolving field of cardiovascular medicine. Computational models serve as critical tools, aiding clinicians in visualizing and understanding arterial behaviors, especially when creating surgical plans (Lashkarinia et al., 2018; Aslan et al., 2022; Liu et al., 2022), predicting growth remodeling (Lashkarinia et al., 2021), and making patient-specific clinical decisions regarding treatment strategies. Patient-specific computational models offer a comprehensive insight into the intricacies of the cardiovascular system, paving the way for more effective and safer surgical interventions.

Among the various modeling techniques, finite element (FE) analysis is notable for the ability to simulate complex mechanical behaviors. FE modeling is widely used for various cardiovascular applications, including simulating an artery pre- and post-surgery,

creating patient-specific designs of stents (Caimi et al., 2018; He et al., 2019; Razaghi et al., 2018), grafts (Fegan et al., 2022), and patches (Lashkarinia et al., 2018; Lashkarinia et al., 2021) for virtual surgical planning, visualizing surgical outcomes, and predicting the mechanical behavior of the repaired or reconstructed artery (Lashkarinia et al., 2018). A variety of constitutive models have been developed to describe the stress-strain response of the arterial wall, such as the Ogden (Ogden, 1972), Fung (Fung, 1967), and Holzapfel-Gasser-Ogden (HGO) (Gasser et al., 2006) models. Experimental studies, including inflation (Sanders et al., 2020), uniaxial, and biaxial tests (Azadani et al., 2012), have been conducted to understand the behavior of arteries and to develop these constitutive models. Arterial walls exhibit a highly nonlinear behavior (Hoffman et al., 2017) and are composed of 3 layers: intima, media, and adventitia. The mechanical properties of arterial walls significantly vary based on the species, age, health, and anatomy (Hayashi, 2003). Therefore, the FE models must account for these variances to accurately simulate the behavior of arterial walls in both unloaded and loaded states (Humphrey, 1995).

In previous research, patient-specific FE models for pulmonary artery (PA) walls were developed to understand the mechanical and structural changes in PAs using invasive measurements and Magnetic Resonance Imaging (MRI) *in vivo* (Lashkarinia et al., 2018; Pourmodheji et al., 2021). However, these studies had limitations due to the assumption of constant thickness or uniform material properties along the arteries. The main challenges faced by FE modeling include uncertainty in the artery wall thickness and material properties. These properties exhibit significant intra- and inter-subject variability and are challenging to measure *in vivo*. The effects of these uncertainties, along with various modeling assumptions, on the mechanical behavior of specimen-specific PA models remain unclear.

In this paper, we developed an FE model to simulate the behavior of PA in a 14-week-old pig model using *in vivo* MRI data. Our aim is to identify the key features of the computational model that accurately capture the spatially-varying deformation response of the vessel walls during the cardiac cycle. We used a well-known HGO model to describe the stress-strain response of the PA walls. In our study, we undertook a stepwise approach to modeling the behavior of the PA walls using FE methods. We began with a simple representation, treating the PA walls as a single-layered structure. This was then expanded to a more intricate two-layered model with different material properties, yet kept the thickness constant across the PA. We introduced further refinement by adjusting the thickness and material properties in distinct PA regions based on *ex vivo* measurements from porcine PAs (Pillalamarri et al., 2021). We aimed to simulate the deformation response of the PA walls under a pressure change, specifically a 13 mmHg increase from diastole to systole (Mueller-Graf et al., 2021). To understand the robustness of the model, we varied its parameters within their standard deviation and analyzed the subsequent impact on deformation.

Our findings demonstrated the necessity of wall thickness gradients, especially from the ventricle towards the lungs, to capture observed arterial wall deformation in-vivo. We also noted a pronounced sensitivity in the pressure-strain response to wall thickness and the isotropic shear modulus. Based on these findings, we adjusted the shear modulus in our porcine models (n=3), striving for a match within 10% of MRI-measured deformations during the cardiac cycle. Our study offers valuable insights into the complexities of modeling and parameter adjustments required for individualized computational artery simulations, setting a foundation for advanced soft tissue deformation simulations. It aims to improve surgical planning, enhance predictions of disease progression, and inform clinical decisions related to treatment approaches.

2 METHODS

Our methodology is outlined in Fig. 1. We first obtained three-dimensional (3D) geometries of a porcine PAs *in vivo* at both peak systole and end diastole, then generated circumferential curves on its surface along the centerline (Fig. 1a). Using the PA geometry at the diastolic state, a computational model was constructed by imposing boundary conditions simulating the increase to peak systolic pressure (Fig. 1b). Once the geometry underwent deformation, we analyzed the deformation pattern throughout the PAs (Fig. 1c) and plotted circumferential strain patterns along the centerline of the PAs. We tuned the model parameters to mimic the strain pattern observed in-vivo MRI measurements (Fig. 1d). We included three porcine models to demonstrate the results of specimen-specific tuning. Further specifics of these procedures are detailed in the subsequent sections.

2.1 Acquisition of In-Vivo PA Geometry

The data were acquired as part of an Institutional Animal Care & Use Committee (IACUC) approved study.

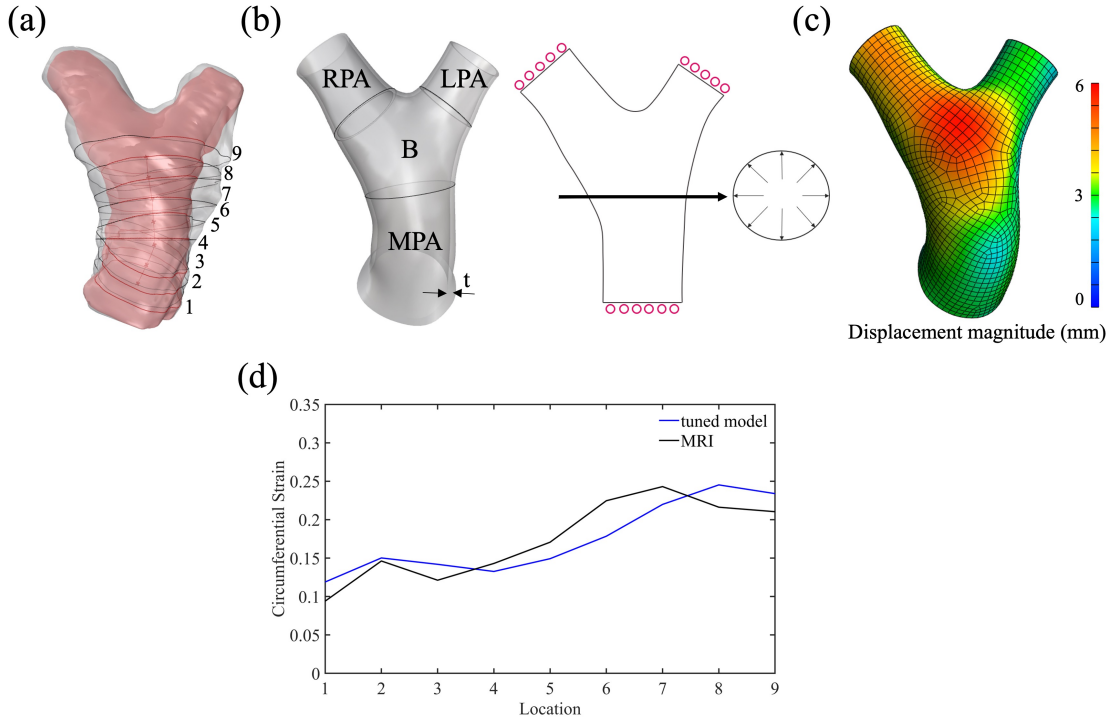

Figure 1: (a) Acquisition of *in vivo* PA geometries (b) Computational model of PA. The solid model was created as thin wall with a thickness, t. Fixed normal displacements were applied at the distal surfaces of MPA, LPA, and RPA, and pressure was applied at the luminal surface along PAs. (c) Resulting displacement magnitude along the geometry. (d) The comparison between strain obtained from tuned model and MRI data.

Magnetic resonance imaging (MRI) was used to obtain the images of PA from three 14-week-old porcine. The segmentation of images was performed using Mimics software (Materialise, Leuven, Belgium) to create 3D anatomies at end-diastole and at peak systole as shown in Fig. 1a in pink and grey, respectively. Nine circumferential curves in the normal directions (Fig. 1a) to the centerline were created on the luminal surface of the PAs. The lengths of the curves were measured from the geometries (at peak systole and end diastole) to estimate the circumferential strain as the difference in circumference normalized by the circumference at diastole.

2.2 Computational Model of the PA

A solid model of the luminal surface at the diastolic pressure was reconstructed from magnetic resonance (MRI) using Rhino3D (McNeel and Associates). The PA wall model included main PA (MPA), bifurcation region B, left PA branch (LPA), and right PA branch (RPA), as shown in Fig. 1b. The walls were created by extruding the luminal surface in the normal direction.

In reality, PA walls consist of three layers: the innermost layer (intima), the middle layer (media), and the outermost layer (adventitia) (Gasser et al., 2006). Previous studies have measured the thickness of these layers in various regions of PAs using ex-vivo samples (Pillalamarri et al., 2021). They also conducted uniaxial and biaxial tension tests (Lally et al., 2004), as well as inflation tests (Boekhoven et al., 2016), to determine the material properties of the walls. Because separating the layers can be challenging, the intima and media (IM) are often tested together after adventitia (ADV) is separated (Tian and Chester, 2012).

In our modeling approach shown in Fig. 2, we introduced varying degrees of complexity to represent the walls. Our geometries include 1 layer (IM) of constant thickness (Fig.2a), 2 layers (IM and ADV) of constant thicknesses (Fig.2b), 1 layer of varying thickness (Fig.2c), and 1 layer of varying thickness with varying material properties (Fig.2d) along the PAs. The material properties used in models in Fig.2 a, b, and c were adapted from (Pillalamarri et al., 2021) from the region designated as MPA-M in their study. In the dual-layer model (Fig2.b), ADV and IM had specific properties. In the model shown in Fig.2d, the region-specific parameters (i.e. MPA, B, LPA, RPA) were adapted from the same study.

The solid model was discretized using trilinear

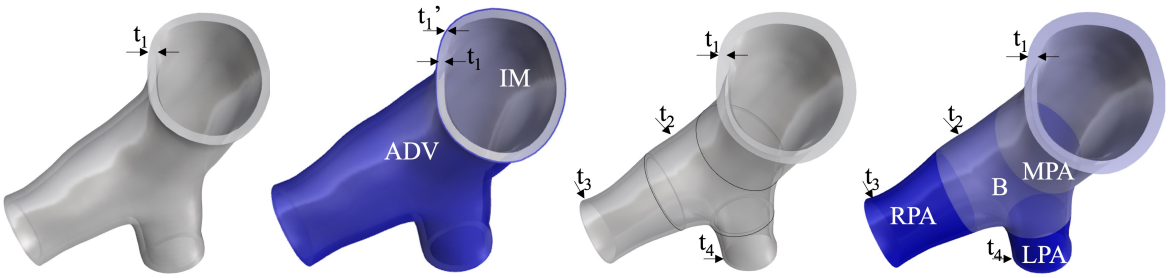

1 layer, constant t	2 layers, constant t	1 layer, varying t	1 layer, varying t, varying materials
t_1=1.41	t_1=1.19, t_1'=0.22	t_1=1.41, t_2=1.03, t_3=0.57, t_4=0.65	t_1=1.41, t_2=1.03, t_3=0.57, t_4=0.65
(a)	(b)	(c)	(d)

Figure 2: Computational models with different wall layers and thicknesses. The unit of thickness is mm.

hexahedral elements using Cubit (v.2023.4 Coreform). The well-established (HGO) model (Gasser et al., 2006), given in equations (1), (2) and (3) for the strain energy density was used to describe the anisotropic elastic stress-strain response of the walls. We used the HGO model parameters determined by ex-vivo tests of porcine PAs by (Pillalamarri et al., 2021). In the equations, Ψ represents strain energy with an isotropic, Ψ_{iso}, and an anisotropic, Ψ_{aniso}, contribution. $\overline{C}$ is the isochoric Cauchy-Green deformation tensor, a_{01} and a_{02} vectors represent the orientations of the collagen fiber families, c is the shear modulus of the isotropic matrix composed of the non-fibrillar components of the PA wall, and k_1 and k_2 characterize the exponential behavior of the collagen fibers.

The average pressure difference between peak systole and end diastole was measured as 13 mmHg in previous porcine studies (Mueller-Graf et al., 2021), therefore, a 13 mmHg pressure was applied to the luminal surface to simulate the increase in blood pressure from the diastolic to the systolic phase. The displacement of the proximal surface of the MPA and the distal surface of the LPA and RPA were fixed in the normal direction. FeBio software was utilized to solve the equations and perform FE simulations using the time step size of 0.1 seconds for 10 time steps.

$$\Psi = \Psi_{iso}(\overline{C}) + \Psi_{aniso}(\overline{C}, \mathrm{a}_{01}, \mathrm{a}_{02}) \tag{1}$$

$$\Psi_{iso} = \frac{c}{2}(\mathrm{I}_1 - 3) \tag{2}$$

$$\Psi_{aniso} = \sum_{layer=M,A} \sum_{i=4,6} \frac{k_1}{2k_2} \left\{ exp\left[k_2 \left(\mathrm{I}_i^{layer} - 1 \right)^2 \right] - 1 \right\} \tag{3}$$

2.3 Postprocessing and Comparison of Deformations

The pressurized geometry was exported in stereolithography (STL) format. The curves on the inner luminal surface along the centerline of PAs were created and their lengths were measured. The percent difference in curve lengths between original model and deformed model was measured as circumferential strain using:

$$\frac{\text{curve length}_{deformed} - \text{curve length}_{original}}{2(\text{curve length}_{deformed} + \text{curve length}_{original})} \tag{4}$$

The results were compared against measured strains from MRI data at the same locations to determine the level of complexity required to capture the strain trend along PAs.

3 RESULTS

3.1 Comparison of Different Computational Models

The circumferential strains along the centerlines of MPA and B regions obtained using different models (Fig.2) are compared in Fig.3.

The difference in circumferential strains between the single-layer and two-layer models, with constant material properties, was negligible. The deformation decreased along the centerline, transitioning from MPA to B when a uniform thickness was applied throughout the PAs. Contrarily, when comparing with MRI-derived strain results, the trend was reversed. Consequently, models with a constant thickness fail

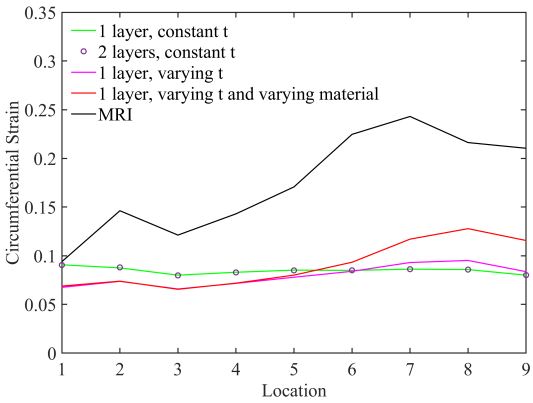

Figure 3: Comparison of circumferential strain results in MPA and B regions using different models. The x-axis indicates the locations where the circumferential lengths were measured on the wall surface along the centerline.

to accurately represent the *in vivo* deformation of the PA walls.

Varying the wall thickness along the centerline, decreasing from MPA to the branches, produced the increasing strain variation congruently with MRI measurements, as depicted by the pink line in Fig.3. Moreover, when material properties were varied along with wall thickness, the strain outcomes increasingly resemble the MRI-measured strain trend, represented by the red line in Fig.3. While the overall trend remains consistent, they were still consistently lower than those measured by MRI across all regions.

The aforementioned results indicated that the experimentally measured regional variation in thickness and material properties are essential for capturing the spatial variation in the pressure-strain response of the PA. Adjusting and fine-tuning the material properties can bring us closer to strains measured *in vivo*, allowing for a more accurate depiction of the mechanical behavior of PA walls across different regions.

The HGO model contains 4 parameters, and it is essential to understand the sensitivity of the pressure-strain response to the model parameters. In the subsequent section, we highlight the sensitivity of strain results to the thickness t, and the HGO model parameters: shear modulus of the isotropic matrix (non-fibrous components of the arterial wall) c, tensile modulus of the collagen fibers k_1, the strain-stiffening parameter of the collagen fiber k_2, and fiber orientation angle β, prior to fine-tuning these to more closely match MRI data.

3.2 Effect of Input Parameters on Deformation

The ranges for PA wall thickness and parameters within the HGO model, specified as mean $\pm$ standard deviation (STD), were obtained from (Pillalamarri et al., 2021). We used the HGO model parameters for region B (as detailed in Table 1) to perform the simulations for investigating the impact of input parameters on deformations. The wall thicknesses for regions B, LPA, and RPA were varied to maintain a consistent standard deviation percentage from the mean, mirroring that of the MPA region. The thickness value in Table 1 corresponds to the MPA, and a proportional adjustment was made for B, LPA, and RPA regions. We performed simulations by applying the same pressure across all the models, and subsequently analyzed the resulting circumferential strains.

	mean	standard deviation
t (mm)	1.19	0.52
C (kPa)	30.03	11.52
k_1 (kPa)	80.73	58.53
k_2	0.67	0.77
β (degree)	55.24	28.71

Table 1: The HGO model parameters adapted from (Pillalamarri et al., 2021). The values for each parameter were varied within their standard deviation.

Input parameters were varied between their high (mean+STD) and low (mean-STD) values one by one and the resulting differences in circumferential strains were plotted in Fig.4. As seen in the plot, the circumferential strain is highly sensitive to the changes in the thickness t and the isotropic shear matrix C, and less sensitive to the changes in k_1, k_2, and β. The parameter k_2 has the least effect on the deformation.

The circumferential strains along the centerline of MPA, B, LPA, and RPA regions were plotted to show the effect of varying input parameters individually in Fig.5. The MRI strains were also included in the figure (bottom right) for comparison of strain trends. The strains obtained with mean values of all parameters were able to capture a similar trend as MRI in MPA and B regions. However, in LPA and RPA regions, trends look significantly different. Specifically, the trend in RPA region suggests an adjustment of thickness to mimic the behavior of PA walls.

3.3 Model Parameter Tuning for Porcine Pulmonary Arteries

We identified that the circumferential strain is most sensitive to the changes in the isotropic shear modulus

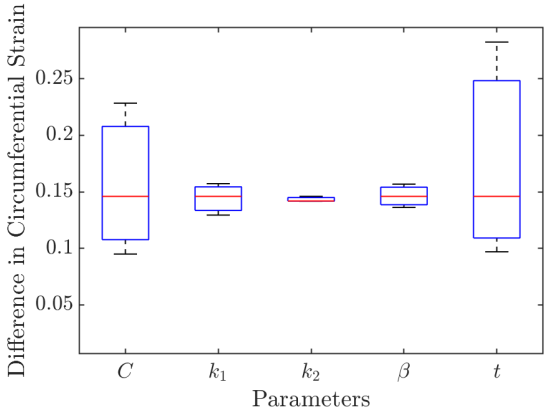

Figure 4: The difference in circumferential strain resulting from changes in parameters between their high and low values.

C and thickness from our analysis in the previous section. We also found that the thickness should be varied to change the strain trend along the PAs from comparing the models with different complexities. Based on these findings, we first tuned the thickness to obtain a more accurate strain trend. We then varied C, which had a scaling effect on the strain trend. The iterative process continued until the difference between predicted and MRI-measured circumferential strains was less than 10 percent. The initial and tuned thicknesses along the PAs are shown in Fig.6. The initial and tuned C values are listed in Table 2 in each region.

	C		
	initial	tuned	range
MPA	40	34	40.77±11.02
B	30	21	30.03±11.52
LPA	43	60	43.24±71.72
RPA	82	80	82.61±90.54

Table 2

A closer match to MRI strains was obtained as a result of the iterative tuning process and demonstrated in Fig.7. We repeated the same process for two additional porcine models. The results are demonstrated in Fig.8. All tuned models show good agreement with the MRI results by reproducing similar strain spatial variation and magnitude. For the three porcine models, the mean discrepancies between the tuned and MRI-measured circumferential strains were 0.035±0.043 in the MPA and B region, 0.009±0.016 in the LPA region, and 0.011±0.045 in the RPA region.

4 DISCUSSION

In this paper, we explored the complexity of computational models necessary for accurate modeling of arterial walls. We also investigated the effects of model parameters on deformations by simulating the pressure increase from end-diastole to peak systole in a porcine PA. Our findings indicate that wall thickness and shear matrix, C, have a notably greater impact on deformation outcomes than other HGO model parameters. We showed that wall thickness variation along the PAs is necessary to accurately mimic the mechanical response of arterial walls. By tuning the input parameters to which the model is highly sensitive, we replicated the in-vivo deformations.

The tuning of input parameters was performed in an iterative manner. The final values we settled on might not yield the smallest discrepancy against MRI, implying that additional tuning might further enhance deformation predictions. In subsequent research, we intend to incorporate an optimization component into our framework for improved predictions.

In our simulations, we applied a 13 mmHg pressure difference between peak systole and end diastole to the inner luminal surface of the walls. This value was sourced from the mean measurement across 10 porcine in a prior study (Mueller-Graf et al., 2021), due to the absence of invasive measurements on our part. Despite this limitation, our findings retain their importance. With access to pressure measurements alongside patient-specific images, prediction accuracy could be further enhanced.

Our computational framework for arterial modeling can enhance surgical planning and inform clinical decisions. In instances like artery reconstruction, suboptimal outcomes or complications may arise from post-surgical shape deformations. The model has the potential to predict these shape changes pre-surgery. We aim to validate our model using post-surgical results of a reconstructed artery in a future study. In the future, as we gain access to detailed material properties of the human arteries through advanced mechanical testing, it will become feasible to translate these specimen-specific porcine models into patient-specific models. This transition will enable a more accurate approach to the personalized treatment of vascular conditions in patients.

5 CONCLUSIONS

This study investigated the complexity required for computational models to predict specimen-specific in-vivo deformations of arterial walls and explored

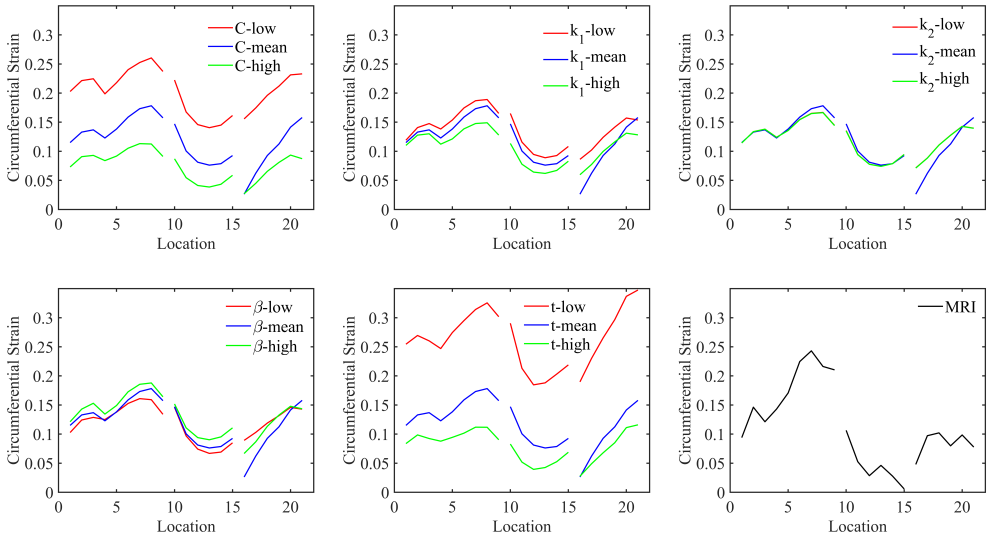

Figure 5: The effect of varying HGO model parameters and wall thicknesses on circumferential strain along the PAs and the comparison of strain trends against MRI measurements. On x-axis, locations 1 through 9 correspond to MPA and B regions, 10 through 15 correspond to LPA, and 16 through 21 correspond to RPA regions.

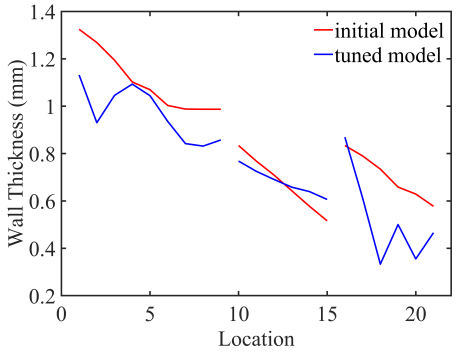

Figure 6: The comparison of wall thicknesses along the centerlines between the initial and tuned model.

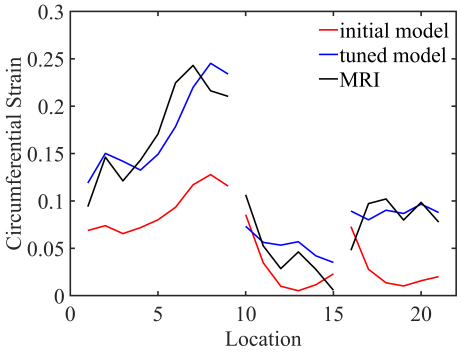

Figure 7: The circumferential strains along the centerline of PAs obtained from initial and tuned model compared against MRI-measured strains.

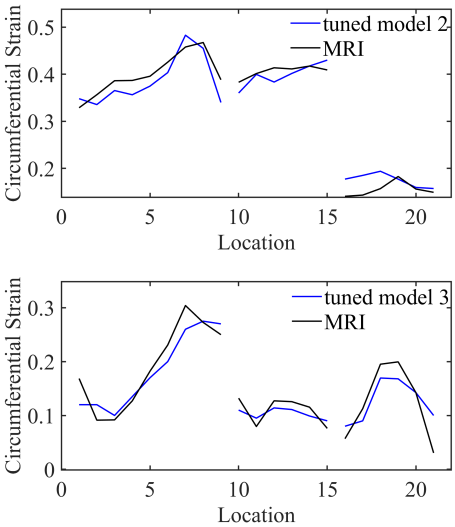

Figure 8: The circumferential strains along the centerline of PAs obtained from tuned models of two additional porcine compared against MRI-measured strains.

the effects of thickness and HGO parameters on deformations. Our findings underscored the importance of varying wall thickness regionally to accurately reproduce MRI-measured strain response in vivo and highlight the significant influence of wall thickness and isotropic shear modulus on strain response results.

Our findings offer valuable insights to identify key

model features for specimen-specific computational modeling of the arteries, thus providing a foundation for enhancing the realism of soft tissue deformation simulations. This enhancement could further improve the outcomes of surgical planning, predictions of disease progression, and clinical decision-making.

ACKNOWLEDGEMENTS

This work was supported by the National Science Foundation under Award NSF FRR CAREER 2144348.

REFERENCES

Aslan, S., Liu, X., Wu, Q., Mass, P., Loke, Y.-H., Hibino, N., Olivieri, L., and Krieger, A. (2022). Virtual planning and simulation of coarctation repair in hypoplastic aortic arches: is fixing the coarctation alone enough? In *BIOINFORMATICS*, pages 138–143.

Azadani, A. N., Chitsaz, S., Matthews, P. B., Jaussaud, N., Leung, J., Wisneski, A., Ge, L., and Tseng, E. E. (2012). Biomechanical comparison of human pulmonary and aortic roots. *European journal of cardiothoracic surgery*, 41(5):1111–1116.

Boekhoven, R. W., Peters, M. F., Rutten, M. C., van Sambeek, M. R., van de Vosse, F. N., and Lopata, R. G. (2016). Inflation and bi-axial tensile testing of healthy porcineácarotid arteries. *Ultrasound in Medicine & Biology*, 42(2):574–585.

Caimi, A., Sturla, F., Pluchinotta, F. R., Giugno, L., Secchi, F., Votta, E., Carminati, M., and Redaelli, A. (2018). Prediction of stenting related adverse events through patient-specific finite element modelling. *Journal of Biomechanics*, 79:135–146.

Fegan, K. L., Green, N. C., Britton, M. M., Iqbal, A. J., and Thomas-Seale, L. E. (2022). Design and simulation of the biomechanics of multi-layered composite poly (vinyl alcohol) coronary artery grafts. *Frontiers in cardiovascular medicine*, 9:883179.

Fung, Y. (1967). Elasticity of soft tissues in simple elongation. *American Journal of Physiology-Legacy Content*, 213(6):1532–1544.

Gasser, T. C., Ogden, R. W., and Holzapfel, G. A. (2006). Hyperelastic modelling of arterial layers with distributed collagen fibre orientations. *Journal of the royal society interface*, 3(6):15–35.

Hayashi, K. (2003). Mechanical properties of soft tissues and arterial walls. In *Biomechanics of soft tissue in cardiovascular systems*, pages 15–64. Springer.

He, R., Zhao, L., Silberschmidt, V. V., Liu, Y., and Vogt, F. (2019). Finite element modelling of stent deployment in a patient-specific coronary artery. *Procedia Structural Integrity*, 15:28–32.

Hoffman, A. H., Teng, Z., Zheng, J., Wu, Z., Woodard, P. K., Billiar, K. L., Wang, L., and Tang, D. (2017). Stiffness properties of adventitia, media, and full thickness human atherosclerotic carotid arteries in the axial and circumferential directions. *Journal of biomechanical engineering*, 139(12):124501.

Humphrey, J. D. (1995). Mechanics of the arterial wall: review and directions. *Critical Reviews™ in Biomedical Engineering*, 23(1-2).

Lally, C., Reid, A., and Prendergast, P. J. (2004). Elastic behavior of porcine coronary artery tissue under uniaxial and equibiaxial tension. *Annals of biomedical engineering*, 32:1355–1364.

Lashkarinia, S. S., Coban, G., Kose, B., Salihoglu, E., and Pekkan, K. (2021). Computational modeling of vascular growth in patient-specific pulmonary arterial patch reconstructions. *Journal of Biomechanics*, 117:110274.

Lashkarinia, S. S., Piskin, S., Bozkaya, T. A., Salihoglu, E., Yerebakan, C., and Pekkan, K. (2018). Computational pre-surgical planning of arterial patch reconstruction: parametric limits and in vitro validation. *Annals of biomedical engineering*, 46:1292–1308.

Liu, X., Hibino, N., Loke, Y.-H., Kim, B., Mass, P., Fuge, M. D., Olivieri, L., and Krieger, A. (2022). Surgical planning and optimization of patient-specific fontan grafts with uncertain post-operative boundary conditions and anastomosis displacement. *IEEE Transactions on Biomedical Engineering*, 69(11):3472–3483.

Mueller-Graf, F., Merz, J., Bandorf, T., Albus, C. F., Henkel, M., Krukewitt, L., Kuehn, V., Reuter, S., Vollmar, B., Pulletz, S., et al. (2021). Correlation of pulse wave transit time with pulmonary artery pressure in a porcine model of pulmonary hypertension. *Biomedicines*, 9(9):1212.

Ogden, R. W. (1972). Large deformation isotropic elasticity–on the correlation of theory and experiment for incompressible rubberlike solids. *Proceedings of the Royal Society of London. A. Mathematical and Physical Sciences*, 326(1567):565–584.

Pillalamarri, N. R., Patnaik, S. S., Piskin, S., Gueldner, P., and Finol, E. A. (2021). Ex vivo regional mechanical characterization of porcine pulmonary arteries. *Experimental mechanics*, 61:285–303.

Pourmodheji, R., Jiang, Z., Tossas-Betancourt, C., Figueroa, C. A., Baek, S., and Lee, L.-C. (2021). Inverse modeling framework for characterizing patient-specific microstructural changes in the pulmonary arteries. *journal of the mechanical behavior of biomedical materials*, 119:104448.

Razaghi, R., Karimi, A., and Taheri, R. A. (2018). Patient-specific finite element model of coronary artery stenting. *Current pharmaceutical design*, 24(37):4492–4502.

Sanders, S. N., Lopata, R. G., van Breemen, L. C., van de Vosse, F. N., and Rutten, M. C. (2020). A novel technique for the assessment of mechanical properties of vascular tissue. *Biomechanics and Modeling in Mechanobiology*, 19:1585–1594.

Tian, L. and Chester, N. C. (2012). In vivo and in vitro measurements of pulmonary arterial stiffness: a brief review. *Pulmonary circulation*, 2(4):505–517.